17

Modeling and Simulation of Microscale Flows

Auro Ashish Saha and Sushanta K. Mitra[1]
Department of Mechanical Engineering, Indian Institute of Technology Bombay, Mumbai India

Abstract

Modeling and simulation are very powerful tools and have become an integral part in the design and development of engineering systems. In the microscale domain, modeling and simulation have been applied in the development of microfluidic devices. Microdevices developed for sample mixing, sample dispersion, drug discovery, biochemical analysis and micropower systems have become possible only due to the impetus and insight gained from the simulation studies of fundamental microfluidic problems. Microfluidic device modeling comprises of dealing with interplay of multiphysics phenomena such as fluid flow, structure, surface and interfaces, etc. As the surface area to volume ratio increases with the decrease of the system feature size of microdevices, some physical phenomena which are insignificant in the macro domain become prominent in the micro domain. Some of the tried and tested macroscale theory and experimental results no longer show similar trends in the microscale. Hence dealing with simultaneously widely differing physics becomes too complicated in the microscale which include microfluidics, microtransport, microthermal, micromechanics, microlectronics and optics with biochemical thermodynamics and reaction kinetics. In this article, the use of numerical modeling and simulation techniques for flow in microchannels applied to microfluidic devices are presented encompassing all the relevant physics at the microscale by the state of the art multiphysics simulation tools such as CFD-ACE+, COMSOL, Fluent to name a few. Numerical simulation of electroosmotic effect on pressure-driven flows in the serpentine channel of a microfuel cell with variable zeta potential on the side walls is investigated and reported. The Poisson-Boltzmann and Navier-Stokes equations are solved numerically to investigate the electroosmotic driven flow phenomena. It is observed that vortices are developed at the straight portion of the microchannel due to the electroosmosis. Flow control in the serpentine microchannel by regulating the zeta potential at the bend has also been demonstrated. Capillary driven flow in a microchannel with alternate hydrophilic-hydrophobic patterns on the bottom wall is investigated for bioreactor applications. The transient flow is modeled by coupling the incompressible Navier-Stokes equation with the interface evolution equation using volume of fluid (VOF) methodology. Higher order surface reconstruction method is adopted for interface tracking. Flow instability increases as the fluid traverses alternately between the hydrophilic and hydrophobic regions. Such flow phenomena in the microchannel indicate that flow control is possible by patterning the channel walls for applications related to

[1] Corresponding Author; Email: skmitra@iitb.ac.in

microfluidic devices. The simulation of dynamic interaction between an elastic membrane structure and fluid in a two-dimensional microchannel is also reported here. The viscous and pressure forces imposed by the fluid flow cause the deformation of elastic membrane which significantly affects the flow field. This involves formulating a coupled fluid structure interaction (FSI) model for the demonstrated case. The solution schemes used for this analysis are based on Lagrangian formulations for the structural parts and Arbitrary Lagrangian Eulerian (ALE) formulations for the fluid regions.
Keywords: Modeling, microchannel, transport, simulation, electroosmotic flow, free surface flow, fluid structure interaction

Nomenclature

Bo	Bond number
Ca	Capillary number
C_0	Ionic concentration in bulk solution
D_h	Hydraulic diameter of channel cross section
d	Diameter of circular top
E	Electric field intensity, elasticity of structure
F	Faraday's constant, liquid volume fraction
F_s	Volumetric force representing the surface tension
H_c	Channel depth
h	Local cell dimension
L	Half length of section of straight segment of channel, channel length
l	Height of structure
n	Normal vector
$\hat{n}$	Unit vector normal to the surface
$\hat{n}_w$	Unit vector normal to the wall
P	Pressure
p	Pressure
Re	Reynolds number
R_c	Radius of curvature of channel axis at U-bend
R_u	Universal gas constant
t	Time
$\hat{t}_w$	Unit vector tangent to the wall
U	Characteristic velocity
u	Velocity component in x-direction
u_{in}	Inlet velocity
V	Velocity vector
V_{inlet}	Velocity of fluid at inlet
v	Velocity component in y-direction, interface velocity
W	Channel height
W_c	Channel width
w	Velocity component in z-direction, width of base structure
z_e	Valance number of univalent fluid
$z_{+/-}$	Valance number of the positive/negative ions in the fluid

Greek symbols

ϵ	Permittivity of fluid
λ	Debye length
μ	Viscosity of fluid
ϕ	Applied potential
ψ	Potential due to electrical double layer
ζ_w	Zeta potential or wall potential
ρ	Density of fluid
ρ_E	Charge density
σ	Surface tension of fluid
θ	Contact angle
η	Viscosity of fluid
κ	Curvature of the surface

Subscripts

c	Channel
in	Inlet
s	Surface tension
w	Wall

1. Introduction

Microfluidics refers to devices and methods for controlling and manipulating fluid flows with length scales less than a millimeter. Microfluidic flows are readily manipulated using many kinds of external fields (pressure, electric, magnetic, capillary, etc.). Microfluidic systems have revolutionized by automation of chemistry and biology, by enabling possibility of numerous experiments performed rapidly and in parallel, while consuming little reagent. A large surface-to-volume ratio is a common characteristic for microfluidics architecture so that, relative importance of surface to volume forces increases. A large surface-to-volume ratio results in the dominance of the viscous effect over the momentum effect. Microfluidic flow is usually a low Reynolds number flow. Fluid/surface interactions become more significant as the dimensions shrinks resulting in a very large surface-tension-driven pressure difference. Flow control is essential in many of the microfluidic systems targeted for use in biochemistry analysis, drug delivery, and sequencing or synthesis of nucleic acids, among others. Such systems use microchannels to promote efficient mixing without the use of any external means. These devices typically rely upon the balance of surface tension and fluid pressure forces to perform their function.

The use of numerical simulation and computational techniques applied to the design and development of microfluidic devices is reviewed here. The transport of pressure-driven, electroosmotic, capillary-driven and flows with fluid structure interaction in microchannels are presented. As microfluidic devices become increasingly complex, it is difficult to perform reliable experiments and hence one needs to rely on numerical tools for optimal fluidic and transport designs. There are a variety of commercially available numerical softwares that have been successfully used in modeling microfluidic devices (eg., COMSOL, CFD-ACE+, Fluent and Coventor). These tools offer multiphysics capabilities which

facilitate the coupling and simultaneous solution of different fundamental equations governing the physics of a given problem.

2. Electrokinetic Flows in Microchannels

Electroosmosis is the motion of fluid caused by externally applied electric potential. In practice, most surfaces contain a residual negative charge. When such charged surface comes in contact with ionizing fluid, the ions having polarity opposite to the surface charge are attracted towards the surface. These ions accumulate near the surface, forming an *electric double layer (EDL).* In this layer ion concentration changes from a maximum value (zeta potential, ζ_w) near the wall to a neutral state in the fluid core. The thickness of this layer is characterized by Debye length, λ, which is defined as the distance from the solid surface to which the charge drops to e^{-1} (37%) of its maximum value. The typical range of zeta potential and Debye length is $20 - 150\ mV$ and $10^{-9} - 10^{-6}$ m, respectively (Brant et al., 2005; Liechty et al., 2005). When electric potential is applied across a capillary, the ions in the EDL move under the influence of the electric field. This ion movement causes bulk fluid motion due to the momentum transfer from EDL to the fluid core.

The convective transport in micro domain is of great importance as it applies to various application such as Micro Electro Mechanical Systems (MEMS) devices, micro-heat exchangers, micro-fuel cells, etc. (Rawool et al., 2006). In fuel cells, the typical fuel such as hydrogen for Proton Exchange Membrane (PEM) or methanol for Direct Methanol Fuel Cell (DMFC), flows through the serpentine flow field present in the bi-polar plates of the cell. Due to the electric potential generated in the micro-fuel cell, a potential gradient is developed in the bi-polar plate, the direction of which is perpendicular to the flow direction. The presence of an aqueous solution in the flow field such as methanol in case of DMFC, results in electroosmosis driven flow, which is of interest for micro-fuel cell applications.

There have been a few studies reported in the field of electroosmosis driven flow in micro DMFC. Karimi and Li (2005) have modeled the electroosmotic flow in the fuel cell membrane including the electrokinetic effect. They have modeled the membrane pore to determine the electroosmotic flow through the membrane for different geometrical and operating conditions. They have reported a nonlinear increase in electroosmotic flow with increase in pore size and found that the electroosmotic drag coefficient increases linearly with pore size.

Several researchers have investigated the effect of varying zeta potential on electroosmotic flow (EOF) in microchannels (Fu et al., 2003; Herr et al., 2000; Chen et al., 2006; Lee et al., 2005; Zhang et al., 2006). Such EOF are in the direction of the pressure driven flow. The characteristics of EOF in a microchannel depend upon the nature of the zeta potential, i.e., whether it is uniform or nonuniform. Fu et al. (2003) used Nernst-Planck equation along with a Navier-Stokes solution to model the EOF that occurs when a step change in zeta potential is applied. The results indicate that a step change in zeta potential causes a significant variation in the velocity profile and also in the pressure distribution.

Microscale debris and manufacturing irregularities during fabrication of microchannels, and adsorption of organics during analysis of microchannels produce nonuniform zeta potential distributions along the channel walls. Herr et al. (2000) have shown the influence of zeta potential on the velocity profile and sample dispersion rate for electroosmotic flow in cylindrical capillaries with nonuniform zeta potential distribution. Similarly, Chen et al.

(2006) investigated numerically the effects of step change in zeta potential in a cylindrical microchannel on electroosmotic flow. It is observed that the variable zeta potential along the flow direction generated regions of positive and negative pressure gradients in the flow field. Lee et al. (2005) studied electroosmotic flow in a cylindrical microchannel with non-uniform zeta potential distribution. They showed formation of distorted electroosmotic velocity profiles and flow circulation resulting from the axial variation of the zeta potential. However, these studies are related to straight microchannels only.

Zhang et al. (2006) studied the two dimensional flow pattern in microchannels with large aspect ratios with heterogeneous zeta potentials, and discuss the formation of secondary EOF's generated by wavelike zeta potential. Their results show that the heterogeneous zeta potentials could generate complex flow patterns and enhance mixing. However, their study may not be representative for microchannels with nearly square cross section.

Souders et al. (2003) have studied combined electroosmotic and pressure driven flows in a three dimensional microchannel with walls covered by charged bands. Under the influence of electroosmotic flow only, it is found that there is a significant amount of fluid folding and stretching. By adding pressure gradient against electroosmotic flow, they showed an increase in the fluid particle residence time. The helical flow structure is also observed for this combined electroosmotic and pressure driven flow.

Fuel feed into the micro fuel cell is an important process affecting its power density and often there is a need to minimize power loss accounting from fuel delivery. Buie et al. (2006) presented a novel design and performance of a planar silicon electroosmotic pump (EO) for methanol fuel delivery in DMFC. Though the EO pump could not deliver enough pressure head for fuel delivery, nevertheless it was interesting to note that the micro DMFC has shown to have improved polarization and power density characteristics with the EO pump. The study in particular emphasizes the performance enhancement due the combined mechanism of electroosmotic phenomena and diffusion for fuel delivery.

Rawool and Mitra (2006) studied the transport of methanol in micro-fuel cell under the applied potential which is perpendicular to the direction of the flow with the side walls of the channels subjected to a constant zeta potential. As observed in the existing literature (Herr et al., 2000; Chen et al., 2006) the zeta potential tend to change along the flow field as the fuel gets consumed in the chemical reaction occurring at the catalyst layer, adjoining the flow channels. The heterogeneous zeta potentials in microchannels can also be achieved through chemical modifications, coupled capillaries and integrated systems (Zhang et al., 2006). Hence, Saha et al. (2007) performed numerical studies to understand the flow behavior in the microchannel of the fuel cell under variable zeta potential conditions.

2.1 Governing Equations

The force acting on ions is accommodated as a body force in Navier-Stokes equation, which reads as

$$\rho(V.\nabla)V = -\nabla P + \mu\nabla^2 V + \rho_E E \tag{1}$$

where ρ_E is the charge density and E is the electric field. For steady flow with constant properties, the continuity equation can be written as

$$\nabla.V = 0 \tag{2}$$

The electric field E in Eqn. (l) has two contributions. One is the field due to applied potential (ϕ) for which governing equation is

$$\nabla^2 \phi = 0 \tag{3}$$

The second contribution is the field due to EDL which is governed by the equation

$$\nabla^2 \psi = -\frac{\rho_E}{\epsilon} \tag{4}$$

The charge density is given by

$$\rho_E = FC_0 z_- e^{(z_- F\psi/R_u T)} - FC_0 z_+ e^{(z_+ F\psi/R_u T)} \tag{5}$$

which, for a symmetric electrolyte of valance number z_e becomes

$$\rho_E = 2FC_0 \sinh\left(\frac{z_e F\psi}{R_u T}\right) \tag{6}$$

where ψ is the potential due to electrical double layer, F is Faraday's constant, R_u is universal gas constant. The Poisson-Boltzmann and Navier-Stokes equations are solved numerically to investigate the electroosmotic driven flow phenomena for prescribed operating conditions.

2.2 Numerical Simulation

Physical Problem

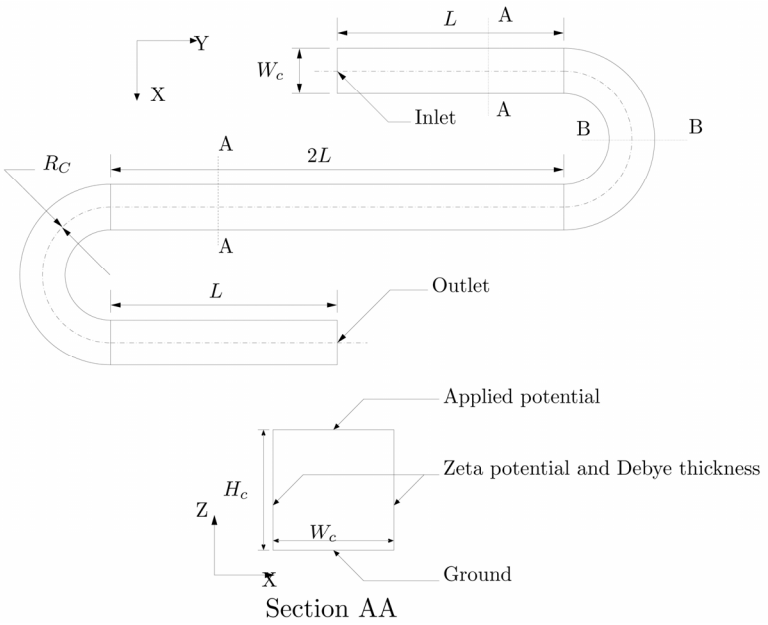

Figure 1. Geometry of serpentine channel

In Fig. 1 schematic of the serpentine microchannel model is shown. The channel considered here is a three dimensional serpentine channel. The cross sectional area of the channel is 100 μm x 100 μm. The model consists of a single 'S' shaped segment of the serpentine channel. It has three straight lengths connected by two semicircular arcs. In Fig. 1 length L = 300 μm and the radius of curvature at bend is R_c = 200 μm.

Boundary Conditions

For fluid flow, a constant velocity corresponding to a given Reynolds number is specified at the channel inlet. At outlet, a constant pressure (atmospheric) is specified. No slip boundary condition is imposed on all the remaining walls. Following is the mathematical representation of the above conditions:

$$\left.\begin{array}{l} u = 0 \\ v = Const. \\ w = 0 \end{array}\right\} \quad \text{for} \quad \left\{\begin{array}{l} 0 < x < 100\ \mu m \\ y = 0 \\ 0 < z < 100\ \mu m \end{array}\right.$$

$$P = 0 \quad \text{for} \quad \left\{\begin{array}{l} 4R_c\ \mu m < x < 4R_c + 100\ \mu m \\ y = 0\ \mu m \\ 0 < z < 100\ \mu m \end{array}\right.$$

$$\left.\begin{array}{l} u = 0 \\ v = 0 \\ w = 0 \end{array}\right\} \quad \text{for all other boundaries}$$

For electric field, a fixed potential is specified at top and bottom walls of the channel, as shown in Fig. 1, which can be expressed as,

$$\phi = 0 \quad \text{Volt} \quad \text{for} \quad \left\{\begin{array}{l} z = 0 \\ \text{for all x and y} \end{array}\right.$$

$$\phi = 0.1 \quad \text{Volt} \quad \text{for} \quad \left\{\begin{array}{l} z = 100\ \mu m \\ \text{for all x and y} \end{array}\right.$$

A zeta potential and Debye length are specified on the side walls of the channel as shown in Fig. 1. The Debye length is kept constant at 1 x 10^{-7} m. The zeta potential is varied linearly on both walls, to investigate the effect of zeta potential profile on the electroosmotic flow. The variable zeta potential condition can be expressed mathematically in the following manner:

$$\zeta_w = -0.01 - \frac{(0.09 - 0.01)}{(100 \times 10^{-6})} Z V \quad \text{for} \quad 0 < z < 100\ \mu m \quad \} \text{ On the left and right wal1}$$

Numerical Technique

The channel geometry is created and meshed using CFD-GEOM modeler. Structured grid is used for simulations. A grid independence study is carried out by successively refining the grid, increasing the number of elements in the domain. The grid is made extra fine in the near wall region where maximum gradients occur. For a grid having 260431 elements, the solution is found to be grid independent. Hence this mesh size was used in all the cases.

CFD software CFD-ACE+ is used for the simulations. Upwind scheme is used in the CGS+Pre solver (ESI CFD Inc., 2006) for velocity and electric field while AMG solver is used for pressure correction. Parametric solver is used to solve for values of inlet velocity corresponding to a range of Reynolds number. A Reynolds number of 0.001 is used in the simulations. Here, Reynolds number is defined as

$$Re = \frac{\rho V_{inlet} D_h}{\mu}$$

where D_h is the hydraulic diameter of the channel, defined as

$$D_h = \frac{4(W_c \times H_c)}{2(W_c + H_c)}$$

Here W_c is the width of the channel and H_c is the depth of the channel as shown in Fig. 1. The effect of zeta potential profile on the velocity profile in the channel is studied. The physical and dielectric properties of methanol at 25° *C* used for simulations are provided in Table 1.

Physical property	Value	Dielectric property	Value
Density *(kg/m³)*	785	Electric conductivity (1/ohm-m)	4.4×10^{-4}
Viscosity *(Pa. s)*	5.6×10^{-4}	Relative permittivity	33.62

Table 1. Properties of methanol

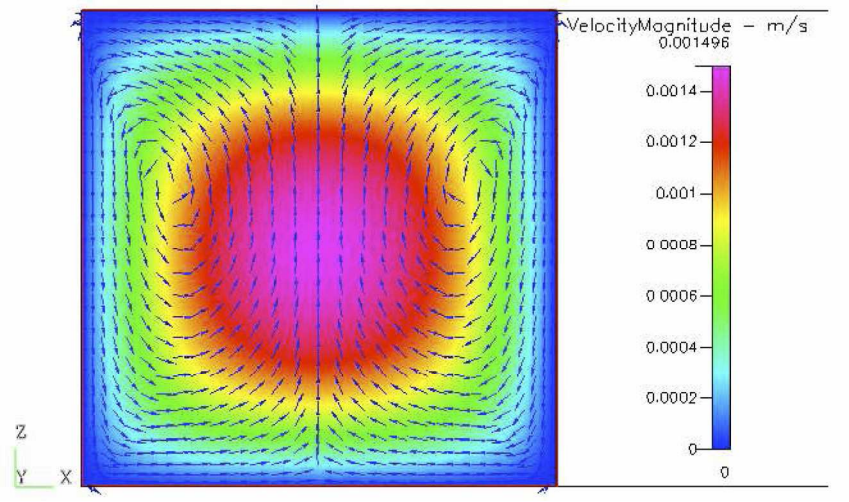

Figure 2. Flow pattern in the channel cross section at 150 μm from channel inlet (section AA in Fig. 1)

Results and Discussion

The velocity vectors in the straight portion of the microchannel, at a distance of 150 μm from the channel inlet, is shown in Fig. 2. The color indicates the velocity magnitude $\sqrt{u^2 + v^2 + w^2}$ while the vectors indicate direction of in-plane component $\sqrt{u^2 + w^2}$. It can be

seen that due to electroosmotic driving force, a secondary vortex pair has been generated in the flow cross section such that the fluid near the side walls moves towards the bottom plate. The fluid again rises in the central portion of the channel to maintain the continuity. Thus two distinct vortices are formed due to electroosmosis. These kind of vortices are absent in case of flow without electroosmosis. This modified flow profile gives rise to additional pressure drop in case of flow with electroosmosis (Rawool & Mitra, 2006). The centers of both the secondary vortices are shifted towards the top wall due to gradual change in the electroosmotic driven force on the fluid as the zeta potential is linearly varied for each wall. This results in shifting of the secondary vortex by a smaller distance. The streamline plot is shown in Fig. 3 which depicts the formation of vortices and the effect of variable zeta potential is clearly seen.

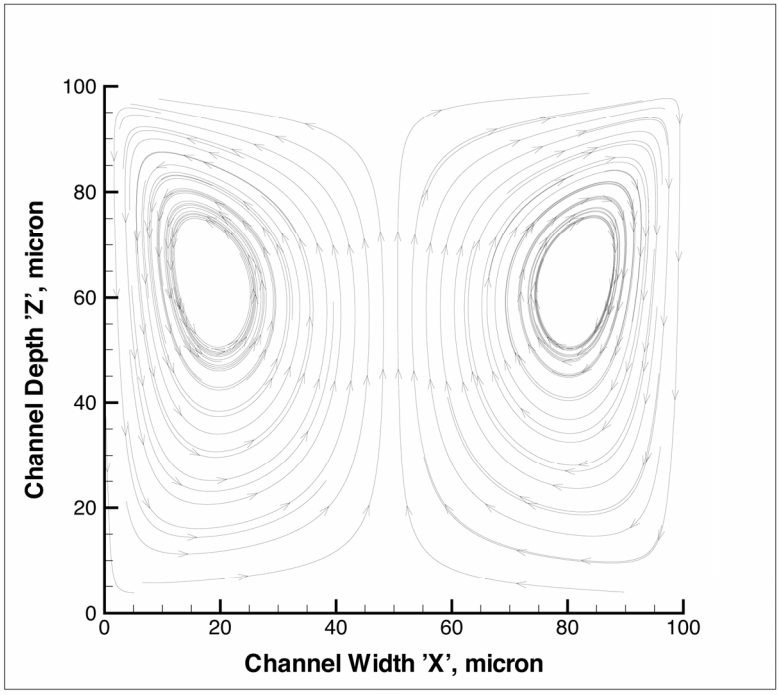

Figure 3. Streamline plot in the channel cross section at 150 μm from channel inlet (section AA in Fig. 1)

The flow behavior at the semi-circular bend for section BB in Fig. 1 has also been studied for four different cases. Figure 4 shows the streamline plots at the bend for pressure driven flow and the applied zeta potential of -0.1 mV, -1 mV and -50 mV, respectively. Fig. 4a shows the formation of vortices purely due to the pressure-driven flow with no contribution from the electroosmotic effect. As the applied zeta potential is increased at the semi-circular bend (section BB in Fig. 1), the electroosmotic forces cause the vortices to shift in a clockwise direction as shown in Fig. 4d. The observed shift of secondary vortices in a clockwise direction with an increase in the applied zeta potential presents an excellent opportunity for obtaining flow control in the serpentine microchannel by regulating the zeta potential at the

bend. Formation of additional vortices at the top left and bottom right corners has also been observed when the applied zeta potential is -0.1 mV, as shown in Fig. 4b.

Figure 5 shows the z component of velocity along the channel width at z = 50 μm for the cross section BB. It is observed here that for a pressure-driven flow only, the z component velocity is zero as the secondary vortices appear at the center line and results in a zero velocity at the central core. It is found that the z component reaches a maximum at a small distance from the wall when zeta potential of -0.1 mV, -1 mV and -50 mV is applied on the side walls. The maximum velocity is reached for the -50 mV of applied zeta potential and decreases in magnitude as the applied zeta potential is reduced. The velocity component then drops to zero and again reaches a maximum value in opposite direction at the center of the channel. Hence, it can be concluded that the z component velocity influences the formation of vortices in the semi-circular bend at the cross section BB and results in the shifting of the vortices in the clockwise direction.

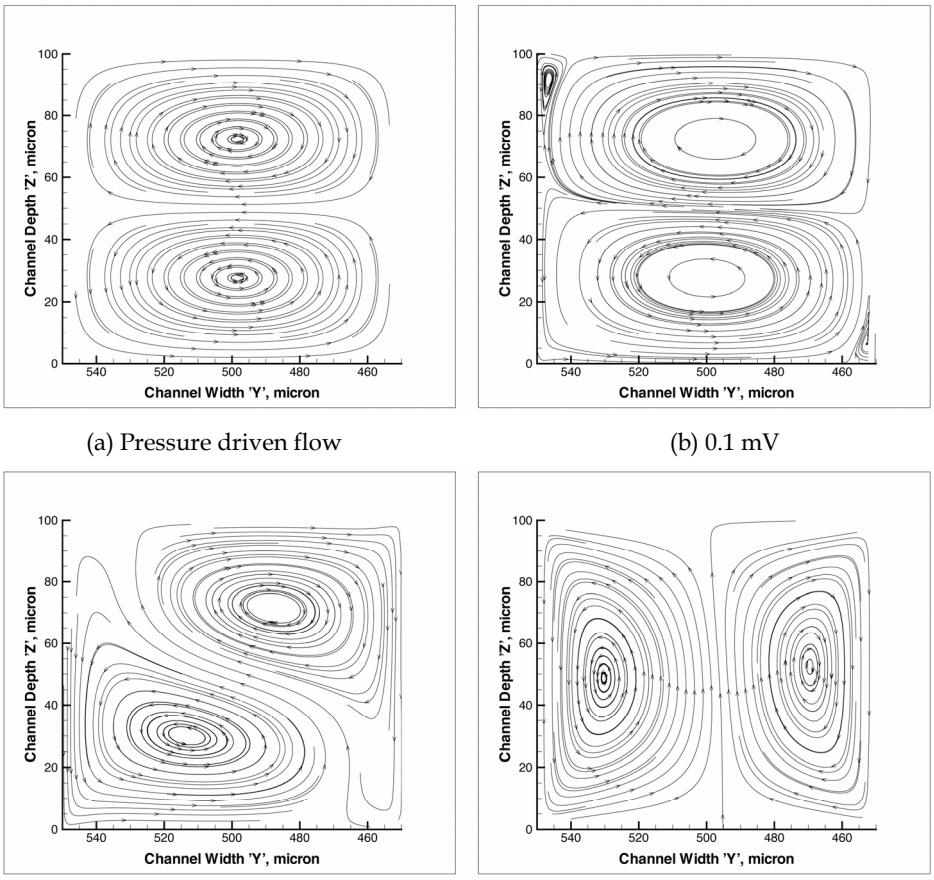

(a) Pressure driven flow (b) 0.1 mV

(c) 1 mV (d) 50 mV

Figure 4. Streamline plots in the channel cross section at the bend (section BB in Fig. 1) for different zeta potential values

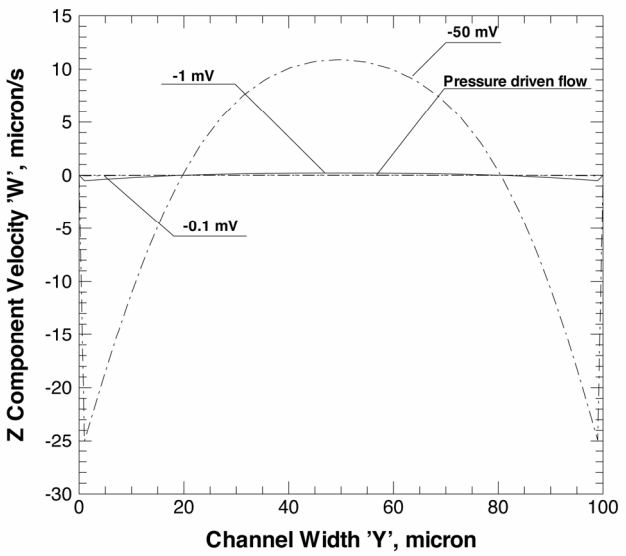

Figure 5. Variation of z component of velocity at $z = 50\ \mu m$ along the channel width at section BB

3. Free Surface Flows in Microchannels

An interface between a gas and liquid is often referred to as a free surface. There are large differences in the densities of the gas and liquid at the interface. The only influence of the gas is the pressure it exerts on the liquid surface and hence the gas-liquid surface is not constrained, but free.

There are three essential features needed to properly model free surfaces: (1) A scheme is needed to describe the shape and location of a surface, (2) An algorithm is required to evolve the shape and location with time, and (3) Free-surface boundary conditions must be applied at the surface. The free surface problem has been formulated by using Lagrangian and Eulerian representation of continuum motion. In Lagrangian algorithms the nodes move with continuum, in Eulerian algorithms the nodes stay in place while the continuum moves through the stationary mesh or through Eulerian coordinate system. Non-Lagrangian algorithms deal with convection (advection) effect. The Lagrangian Grid Methods follow the Lagrangian formulation. The principal limitation of Lagrangian methods is that they cannot track surfaces that break apart or intersect. Arbitrary-Lagrangian-Eulerian (ALE) method exploit the merits of both Lagrangian and Eulerian formulation. Where as, Surface Height Method, Marker-and-Cell (MAC) Method, Surface Marker Method, Volume-of-Fluid (VOF) Method are purely based on Eulerian formulations. In Lagrangian or ALE-approaches, the free-surface always falls on the boundary of the computational domain. Hence, such methods do not pose any additional difficulty in applying complex boundary conditions. However these methods suffer the deficiency of requiring frequent remeshing. The choice of Lagrangian/ALE-method as opposed to VOF-variants, is based mainly on the type of problem and degree of precision to which the resulting free-surface is to be determined

(Sujatha et al., 2006). VOF technique tracks the fraction of each phase in every computational cell to extract the interface shape. The most successful of the various free surface methods is the VOF technique because of its simplicity and robustness.

Manipulating gas and liquid flows within networks of microchannels is crucial in the design and fabrication of microfiuidic devices. As the surface area to volume ratio increases, fluid/surface interactions become more significant with smaller fiuidic channels (Madou, 2002). Research on patterned surfaces revealed interesting phenomena that can be exploited to control liquid motions in microfiuidic devices. Hydrophobic and hydrophilic regions inside microchannels can be patterned through surface modification. However, fabrication of such patterned surfaces with selective surface characteristics is highly challenging task (Deval et al., 2004).

There have been a few studies reported for flow in patterned microchannels. Zhao et al. (2001) used surface directed liquid flow to create pressure sensitive switches inside channel networks. Self assembled monolayer chemistry is used in combination with multi-stream laminar flow and photolithography to pattern surface inside the microchannel networks. Kim et al. (2002) carried out experimental and numerical investigation for microchannel transient filling process with surface tension. A linear relationship between the dimensionless pressure and capillary number is observed. Their experimental observations indicate that flow blockage in the narrowest width channel is enabled by the surface tension and not by viscous effect.

Yang et al. (2004) discuss the method to characterize the surface energy inside a microchannel by monitoring the marching velocity of capillary meniscus. They formulated one-dimensional mathematical model and performed experimental validation of liquid filling in a capillary. Parylene and silicon nitride microchannels, which are fabricated using surface micromachining technology, are used for experimentation. The study indicates the influence of surface tension driven flow for fluid delivery in microfluidic systems.

Salamon et al. (2005) used finite element based numerical method to study a three-dimensional flow of Newtonian fluid in a 80 μm high microchannel with superhydrophobic lower and upper walls. They have shown a 40% flow enhancement over the smooth non-patterned surface and a apparent slip length of 5.4 μm. Byun et al. (2005) performed numerical visualization to investigate the effect of surface wettability in microchannel on the flow characteristics. The importance of hydrophobic and hydrophilic characteristics on a surface for the handling and control of liquid in the micro-systems are emphasised. The study shows the occurrence of flow instability in the flow path when the meniscus crosses hydrophilic/hydrophobic interface. Dalton et al. (2006) discuss issues in implementing superhydrophobic surfaces by nanostructured posts in a microchannel. The understanding and elimination of contact line movement effects on drag reduction is illustrated. Yang and Przekwas (1998) developed the computational methodology to model surface tension effects of multi fluid flow in ACE+MEMS CAD software. They present systematic validations against analytical solution for typical flows in MEMS devices. The unsteady motion of the free surface governed by the Hamilton-Jacobi evolution equation is solved on Eulerian grid using the Volume of Fluid (VOF) technique. Hirt and Nichols (1981) describe the concept of VOF method for treating complicated free boundary configurations. For simulation related to free surface flows, the water/air interface is characterized by surface tension and sharp changes in viscosity and density (Kothe et al., 1996). Among several general multiphase

models currently in use, the VOF model is the only multiphase model that enables identification of the interface clearly (Yian & Lawal, 2006).
Huang et al. (2006) have studied theoretically and numerically the capillary filling flows inside patterned surface microchannels. Two different patterned microchannel configurations - inner walls patterned with unequal contact angles; each inner wall divided into two equal segments having different contact angles have been considered for carrying out two-dimensional and three-dimensional simulations. Equivalent contact angle model based on surface energy method has been proposed for estimating capillary flows inside the patterned surface microchannels and they validated the model with traditional capillary rise theories.
A new method has been developed to modify the hydrophobic and hydrophilic nature of silicon surfaces by the use of 5-(4-Hydroxyphenyl)-10, 15, 20-tetra (p-tolyl) porphyrin self assembled monolayer (SAM) (Nayak et al., 2007; Mitra & Saha, 2008). The bare SiO_2 substrate exhibited a contact angle of 33 ±2° showing hydrophilic nature of the surface. In the case of Hydroxy-phenyl porphyrin SAM, the contact angle is found to increase up to 75 ± 3°, indicating a hydrophobic nature of the surface due to the formation of SAM on the SiO_2 surface.
Saha and Mitra (2007, 2008) presented numerical study on the surface dominated flow behavior in a channel with unsymmetrical distribution of surface characteristics with respect to channel axis. A three-dimensional (3D) numerical simulation of flow in patterned microchannels with alternate hydrophilic and hydrophobic surfaces at the bottom wall is considered. Hydrophilic surface induces the acute static contact angle while hydrophobic surface results in the obtuse static contact angle. Passive capillary driven flow phenomena in the microchannel is considered in their study. Capillary driven flows are purely governed by the forces associated with surface tension (Probstein, 1994) and offer positive flow enhancement effect.

3.1 Governing Equations

VOF Model

The simulations of the capillary flows in the patterned-surface microchannels are performed using a VOF method. In this method, a volume fraction transport equation is employed in addition to the continuity and momentum equations. Two phases (gas-liquid) are treated as a homogeneous gas-liquid mixture. The flow is considered to be laminar, non-gravity, incompressible, Newtonian and isothermal with velocity field V and governed by the Navier-Stokes and continuity equations, as provided here:

$$\nabla . V = 0 \tag{7}$$

$$\frac{\partial \rho V}{\partial t} + \nabla .(\rho VV) = -\nabla P + \nabla .(\mu(\nabla V + \nabla^T V)) + F_s \tag{8}$$

where V is the velocity of the mixture, P the pressure, t the time, F_s the volumetric force at the interface resulting from surface tension, and ρ, μ are the density and viscosity, respectively. In this equation the accumulation and convective momentum terms in every control volume (cell) balance the pressure force, shear force, and additional surface tension force F_s. Surface tension arises as a result of attractive forces between molecules in a fluid and it is represented as force acting only at the surface, which is required to maintain equilibrium in such instances.

The numerical simulation of free surface flows composed of two immiscible fluids involves two coupled tasks namely resolving the flow field and updating the position of the interface. This involves the application of SIMPLE algorithm (Patankar, 1980) and extending it to include the VOF methodology (Hirt & Nichols, 1981; Kothe et al., 1996). VOF method allows for the simulation of a mixture of two incompressible and immiscible fluids including surface tension effects. The VOF model includes the effects of surface tension along the interface between each pair of phases. The model can be augmented by the additional specification of the contact angles between the phases and the walls. The fluids under consideration are DI water as liquid and air as gas. The tracking of the interfaces between the phases is accomplished by the solution of a continuity equation for the volume fraction of any of the phases. The fields for all variables and properties are shared by the phases and represent volume-averaged values, as long as the volume fraction of each of the phases is known at each location. Thus the variables and properties in any given cell either represent one or a mixture of the phases, depending upon the volume fraction values. The distribution of the liquid phase is described by using a single scalar field variable, F, which defines the fraction of the liquid volume. Here, $F = 1$ represents liquid, $F = 0$ represents gas and $0 < F < 1$ represents the liquid/gas interface. The volume fraction distribution can be determined by solving the passive transport equation, given as:

$$\frac{\partial F}{\partial t} + V.\nabla F = 0 \tag{9}$$

where,

$$F = \frac{\text{cell volume occupied by liquid}}{\text{total volume of the control cell}} \tag{10}$$

The mixture's physical properties are derived from that of the two phases through the volume fraction function. In particular, the average value of any volume-specific quantity, ρ in a computational cell can be computed from the value of F in accordance with:

$$\rho = F\rho_2 + (1-F)\rho_1 \tag{11}$$

where the subscripts 1 and 2 represent the gas phase and the liquid phase, respectively. For an intensive quantity, μ, the effect of density can be included as given below:

$$\mu = (F\rho_2\mu_2 + (1-F)\rho_1\mu_1)/(\rho_1 + \rho_2)/2 \tag{12}$$

The surface tension model follows the continuum surface force (CSF) model proposed by Brackbill et al. (1992). The surface tension is specified as a source term F_s in Eq. 8 according to the CSF model:

$$F_s = \frac{\rho\sigma\kappa\nabla F}{(\rho_1 + \rho_2)/2} \tag{13}$$

The surface tension is taken to be constant along the surface and only the forces normal to the interface are considered. According to the CSF model, the surface curvature κ is computed from local gradients in the surface normal to the interface, which is given as:

$$\kappa = \frac{1}{|n|}\left(\left(\frac{n}{|n|}\cdot\nabla\right)|n| - \nabla\cdot n\right) \tag{14}$$

where $n = \nabla.F$ is the normal vector. Wall adhesion is included in the model through the contact angle:

$$\hat{n} = \hat{n}_w \cos\theta + \hat{t}_w \sin\theta \tag{15}$$

where *n* is the unit vector normal to the surface, $\hat{n} = \frac{n}{|n|}$, $\hat{n}_w$ and $\hat{t}_w$ represents the unit vector normal and tangent to the wall, respectively. The interface needs to be constructed based on the computed value of the volume fraction with the application of interpolation schemes for the identification of the interface. An upwind scheme with the piecewise linear interface construction (PLIC) method, is adopted for surface reconstruction (Kothe et al., 1996). In the PLIC scheme, the liquid-gas interface is assumed to be linear and can take any orientation within the cell. The reconstructed interface is represented by line segments in a two-dimensional flow and by an arbitrary polygonal face for three-dimensional flows. The reconstruction is required at every time step to include the necessary back-coupling of surface forces to the momentum equations as well as flux calculations. Equations (7) – (15) are solved iteratively to obtain the liquid volume fraction and the velocity field solution under appropriate initial and boundary conditions.

For the channel height of 100 μm selected in this study, the Bond number (Bo), $\rho g H^2/\sigma$, and Capillary number (Ca), $\mu U/\sigma$, are much less than unity. Hence, the effects of gravity and dynamic contact-angle are not taken into account in the present study.

The solution of the passive transport equation in conjunction with the standard conservation equations in CFD-ACE+ requires three related actions: (1) Compute mixture properties, (2) Reconstruct the fluid-fluid interface in each cell, and (3) Determine the contribution of the secondary fluid flux to the equations for conservation of mass, momentum, energy and volume fraction. The classification of the VOF method as a volume-tracking method follows directly from the use of the single scalar variable F to describe the liquid distribution and to solve for the liquid volume evolution. One consequence of the purely-volumetric representation of the phase distributions is that there is no unique definition of the interface between the two phases. As such, if the location of the interface is required for any modeling, computational, or visualization purpose, then it must be dynamically reconstructed from the F distribution. In CFD-ACE+, surface reconstruction is a prerequisite for determining the flux of fluid two from one cell to the next and for determining surface curvatures when the surface tension model is activated. In the PLIC scheme (Fig. 6), the liquid-gas interface is assumed to be planar and allowed to take any orientation within the cell, and will therefore generally have the shape of an arbitrary polygonal face. The facet in a cell is fully defined by specifying: (i) the spatial orientation of the infinite plane that contains the facet; and, (ii) the location of a point within the cell through which the infinite plane passes. The orientation is specified by specifying the outward-pointing unit normal of the infinite plane, and the sense of the normal is here arbitrarily chosen so that it points out of the liquid phase and into the gas phase. The unit normal of the plane is determined by assuming that it is parallel to the gradient vector of F. The gradient of F is determined from the local distribution of F in a set of cells which includes the target cell and all its immediate

neighbors. The location of the anchor point is determined by finding the infinite cutting plane perpendicular to the unit normal of the infinite plane that truncates the correct liquid volume from the cell, in that it satisfies the condition:

$$V_{cut} = F.V_c \tag{16}$$

where V_{cut} is the volume of the cell truncated by the cutting plane, V_c is the volume of the whole cell, and F is as defined above. In the PLIC scheme, each cell has a unique surface normal that can be used to compute the surface curvature from cell to cell. This calculates and adds surface tension forces for the free surfaces.

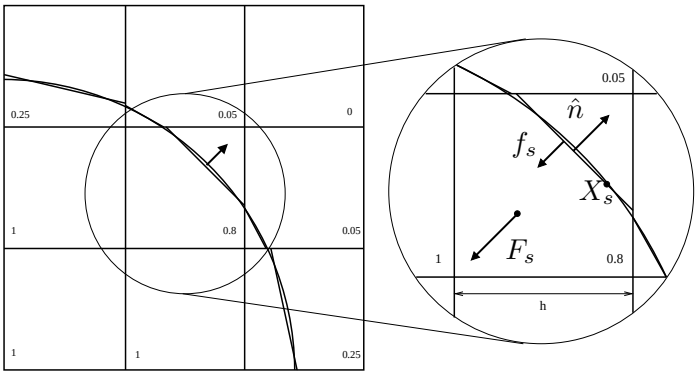

Figure 6. PLIC reconstruction scheme

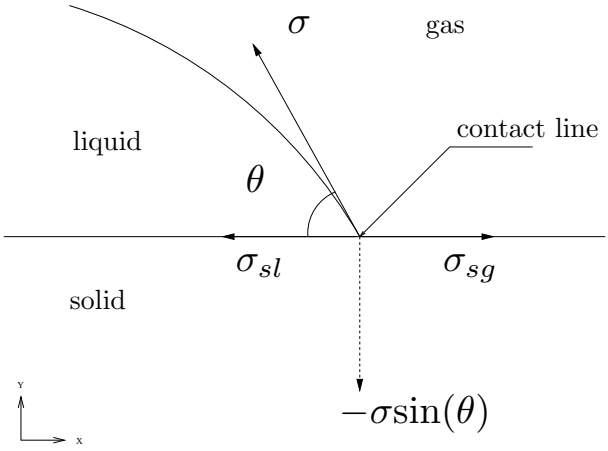

Figure 7. Contact angle

Lucas-Washburn Model

Analytical solution for the propagation of a liquid in a channel is derived in the following sections. The analytical solution is based on the Navier-Stokes equation for incompressible, quasi-steady, laminar, Newtonian 2D horizontal flow,

$$-\frac{\partial P}{\partial x} = -\mu \frac{\partial^2 u}{\partial y^2} \tag{17}$$

where P is the pressure in the fluid at x, μ , is the viscosity of the fluid, u is the velocity of the fluid. For a fully developed capillary driven flow, the analysis on the balance of viscous force, surface tension force, and gravitational force yields the classical Lucas-Washburn equation on the penetration length, L, evolution with time, t (Washburn, 1921).

For static wetting of a liquid between two surfaces, the minimization of surface area of a liquid may result in a curved interface. The general Young's-Laplace equation describes the relation for the pressure difference across the interface as (Fig. 7):

$$\Delta P = \sigma \left(\frac{1}{\mathrm{R}_1} + \frac{1}{\mathrm{R}_2} \right) \tag{18}$$

where ΔP is the pressure difference, σ is the liquid surface tension, and R_1 and R_2 are the radius of curvature of the interface in directions perpendicular and parallel to the liquid stream. For a two-dimensional channel $R_2 = \infty$.

Therefore,

$$\Delta P = \sigma \frac{1}{\mathrm{R}} \tag{19}$$

From Fig. 8,

$$R = \frac{h}{2\cos\theta} \tag{20}$$

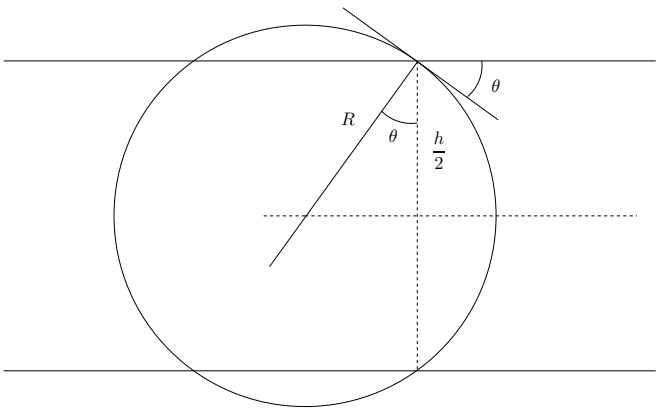

Figure 8. Meniscus in channel

For steady 2D Poiseuille flow,

$$u_{avg} = \frac{1}{12\mu} \frac{\Delta P}{L} h^2 \tag{21}$$